Antarctic Science 25(5), 697–710 (2013) © Antarctic Science Ltd 2013 doi:10.1017/S0954102013000096

Parameterization of clear sky effective emissivity under surface-based temperature inversion at Dome C and South Pole, Antarctica

MAURIZIO BUSETTO[1], CHRISTIAN LANCONELLI[1], MAURO MAZZOLA[1], ANGELO LUPI[1], BOYAN PETKOV[1,2], VITO VITALE[1], CLAUDIO TOMASI[1], PAOLO GRIGIONI[3] and ANDREA PELLEGRINI[3]

[1]*Institute of Atmospheric Sciences and Climate, National Research Council, Via Gobetti 101, 40129 Bologna, Italy*
[2]*International Centre for Theoretical Physics, Strada Costiera 11, 34014 Trieste, Italy*
[3]*Italian National Agency for New Technologies, Energy and Sustainable Economic Development, Via Anguillarese 301, 00123 Roma, Italy*
m.busetto@isac.cnr.it

Abstract: For most parts of the year the Antarctic Plateau has a surface temperature inversion with strength *c.* 20 K. Under such conditions the warmer air at the top of the inversion layer contributes more to the clear sky atmospheric longwave radiation at surface level than does the colder air near the ground. Hence, it is more appropriate to relate longwave irradiance (LWI) to the top of the inversion layer temperature (T_m) than to the ground level temperature (T_g). Analysis of radio soundings carried out at Dome C and South Pole during 2006–08 shows that the temperature at 400 m above the surface (T_{400}) is a good proxy for T_m and is linearly related to T_g with correlation coefficients greater than 0.8. During summer, radiosonde measurements show almost isothermal conditions, hence T_{400} still remains a good proxy for the lower troposphere maximum temperature. A methodology is presented to parameterize the clear sky effective emissivity in terms of the troposphere maximum temperature, using ground temperature measurements. The predicted LWI values for both sites are comparable with those obtained using radiative transfer models, while for Dome C the bias of 0.8 W m^{-2} and the root mean square (RMS) of 6.2 W m^{-2} are lower than those calculated with previously published parametric equations.

Received 18 April 2012, accepted 5 January 2013, first published online 2 April 2013

Key words: BSRN, downwelling longwave irradiance, high Antarctic Plateau, radio sounding

Introduction

Accurate estimations of atmospheric longwave irradiance (LWI) at the surface are important in determining the radiation budget wherever direct measurements are not available. With the aim of providing a longwave radiation climatology that would be useful for validating Global Circulation Model (GCM) computations, King (1996) investigated seasonal and spatial variations of LWI in Antarctica, making use of data supplied by four stations: two representative of the coastal climatological regime (Syowa & Neumayer), one of the Antarctic region characterized by the strong katabatic winds regime (Mizuho), and one of the Antarctic Plateau (South Pole). The study was not able to discern between clear and cloudy-sky conditions because monthly means were used, thus limiting the possibility to investigate the particular characteristics of radiative processes in the Antarctic atmosphere under clear or cloudy-sky conditions separately.

In a cloud-free atmosphere assumed to behave as a grey body, LWI is a function of the vertical profiles of temperature and greenhouse gas concentrations. Since measured vertical profiles of these parameters are not always available for accurate radiative transfer calculations, LWI is usually parameterized in terms of an appropriate temperature, making use of the Stefan-Boltzmann emission law for a grey body:

$$LWI = \varepsilon\sigma T^4, \quad (1)$$

where σ is the Stefan-Boltzmann constant and T is the reference temperature, which requires the definition of an effective atmospheric emissivity ε. Many empirical and physically based formulations have been developed since the pioneering works of Ångström (1918) and Brundt (1932) to describe the relationships between effective clear sky emissivity ε and surface observations of temperature and water vapour content (Swinbank 1963, Idso & Jackson 1969, Ohmura 1982, Zillman 1972, Guest 1998). The success of such methods in representing LWI features strongly depends on the site climatology.

In the presence of a variable thermal gradient in the boundary layer, a parameterization based on ground-level measurements is likely to be erroneous. Gröbner *et al.* (2009) pointed out that parameterizations of clear sky LWI can be considerably improved by making use of an effective atmospheric boundary layer temperature instead of surface temperature. Moreover, using the ground

temperature T_g in Eq. (1) typically produces a daily oscillation of modelled LWI, according to the variations of T_g, which is not usually observed during measurements performed for clear sky conditions, for example at Dome C. Hence, the applicability of previous parameterizations to the extremely cold and dry conditions of the Antarctic Plateau is not obvious due to the presence of a significant and persistent temperature inversion throughout the year except for a short period during the summer (Hudson & Brandt 2005, Genthon *et al*. 2010). The strong and persistent inversion is mainly due to the higher emissivity of the snow surface ε_s, with value very close to one (Warren 1982), with respect to the emissivity of the atmosphere ε_a for clear sky conditions. Considering that during winter the effect of solar radiation is absent, and that typically only 15% of the energy balance at the surface involves latent heat and sensible heat fluxes, Hudson & Brandt (2005) set the relation $\varepsilon_a T_a^4 \approx 0.85\varepsilon_s T_s^4$ between air temperature T_a and the temperature of the snow surface T_s. For a typical value for the $\varepsilon_a \sim 0.6$, this equation implies that $T_a > T_s$.

Accurate measurements of the infrared radiation in polar regions became routinely available with the establishment of the first Baseline Surface Radiation Network (BSRN) sites in the 1990s. Dome C, located on the East Antarctic plateau (75.1°S, 123.3°E, 3233 m above mean sea level), joined this community in 2006 (Lanconelli *et al*. 2011) when continuous measurements of LWI started to be performed routinely at the Italian-French station, Concordia (http://www.concordiabase.eu).

In this study, the LWI measurements collected in the period from January 2006–December 2008 were investigated to determine a suitable parameterization of the clear sky LWI for Dome C. Besides radiation measurements, the one-minute resolved standard meteorological parameters, available from the automatic weather station (AWS) operating at Concordia, and radio sounding measurements, performed every day at 20h00 local time (LT) (12h00 UTC), were used.

Methodology

In most existing parameterizations, atmospheric emissivity ε is expressed as a function of the surface temperature T_g and/or water vapour partial pressure e (Pirazzini *et al*. 2000, Duarte *et al*. 2006). Carrying out accurate measurements of the air relative humidity (RH) in extremely cold regions with standard instruments is difficult. Therefore, considering the extremely dry air-conditions of Dome C (Tomasi *et al*. 2010), we decided to parameterize ε in terms of temperature only. In such a way the estimation of clear sky LWI can be expressed in terms of the following equation:

$$LWI = \varepsilon(T)\sigma T^4, \quad (2)$$

where T is usually assumed to be the air temperature at the surface T_g, also called screen temperature. However, previous studies showed that in the presence of a surface temperature inversion, the temperature at the top of the inversion layer (hereafter T_m, i.e. the maximum temperature) appears more suitable for reproducing LWI clear sky measurements (Yamanouchi & Kawaguchi 1984, King 1996). Considering that T_m is expected to be more stable during the day (Hudson & Brandt 2005, Aristidi *et al*. 2005), the modelled LWI should appear more realistic, being unaffected by the surface temperature oscillations related to the solar radiation cycle.

Wind speed and direction could also affect LWI, because of snow drifting or advection and katabatic flows. At Dome C and South Pole the mean wind speed is much lower than the limit of 13 m s^{-1}, below which drifting snow does not influence the downward longwave flux (Yamanouchi & Kawaguchi 1994), and the region of Dome C is not influenced by katabatic winds. Due to the distance from the coasts (about 1200 km) and the site elevation (3300 m), together with the presence of the polar vortex, the advection from the ocean cannot be easily correlated with wind speed (Udisti *et al*. 2012). For these reasons, we do not use wind data in our LWI parameterization.

Longwave measurements and cloud screening

Downwelling longwave irradiance is continuously measured at Dome C using a pyrgeometer manufactured by Kipp & Zonen (model CG4) calibrated against the World Infrared Standard Group (WISG) hosted at the Physikalisch-Meteorologisches Observatorium Davos/World Radiation Centre (PMOD/WRC), Switzerland. All the measurements are subjected to detailed automatic and manual quality-check procedures, in accordance with BSRN recommendations (Long & Dutton 2002).

The method proposed by Town *et al*. (2007) was used to remove cloud contaminated data. This method (hereafter referred to as scatter plot method) is based on the analysis

Table I. Monthly values of the longwave irradiance (LWI) thresholds used to identify the clear sky situations making use of the scatter plot method, monthly averages of LWI and standard deviations σ_{LWI}, fractions of clear sky periods per month, and number of minutes of LWI valid measurements available in the dataset. SBDART = Santa Barbara Discrete Ordinate Radiative Transfer (DISORT) Atmospheric Radiative Transfer.

	Jan	Feb	Mar	Apr	May	Jun	Jul	Aug	Sep	Oct	Nov	Dec
LWI_{SBDART} (W m^{-2})	109	94	83	79	70	77	71	69	68	74	83	115
LWI (W m^{-2})	109.3	88.2	92.4	79.5	81.8	76.4	75.2	78.5	74.9	77.9	91.4	104.9
σ_{LWI} (W m^{-2})	1.3	0.6	1.1	0.7	1.1	0.8	0.8	0.9	1.2	0.9	0.8	1.1
% clear	59	70	45	51	35	57	52	41	48	56	38	65
N (x 1000)	113	122	132	94	113	121	133	133	129	131	115	131

https://doi.org/10.1017/S0954102013000096 Published online by Cambridge University Press

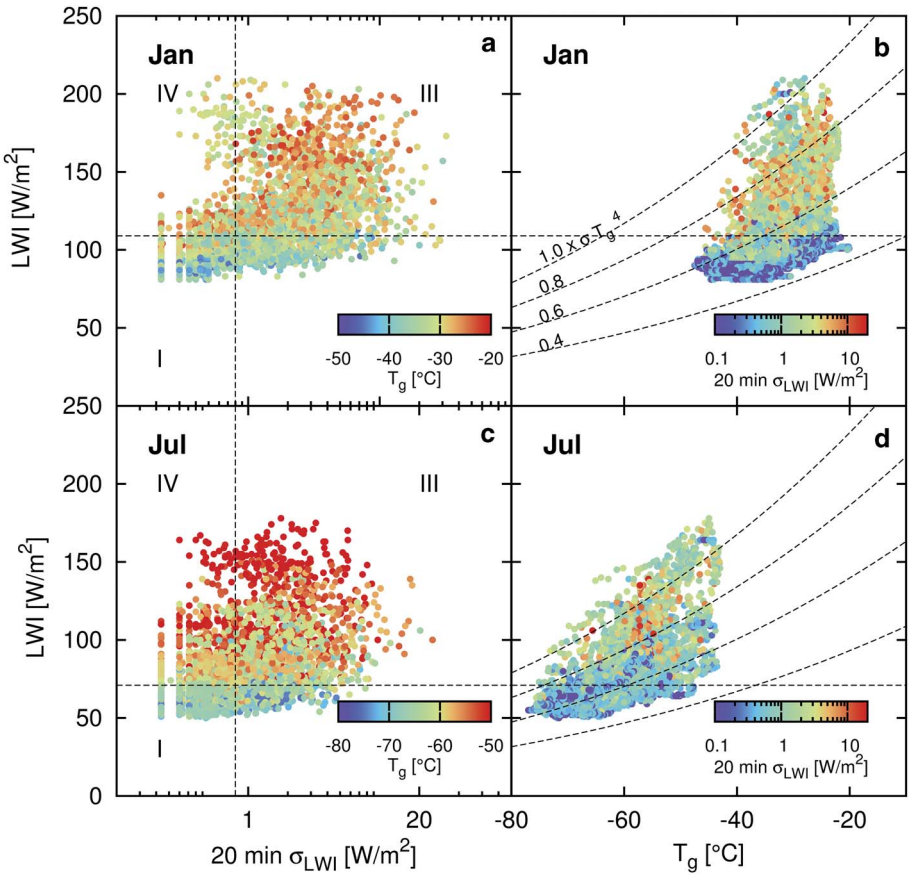

Fig. 1. a. & c. Scatter plots of longwave irradiance (LWI) vs its standard deviation calculated over a 20-min temporal window for the overall January (a.), and July (c.) Dome C data. The thresholds (black dashed lines) for LWI have been calculated by Santa Barbara Discrete Ordinate Radiative Transfer (DISORT) Atmospheric Radiative Transfer (SBDART) using mean monthly profiles of temperature and absolute humidity, while the threshold for standard deviation has been chosen to be 0.8. Clear sky cases are expected to join the quadrant I. **b.** & **d.** The same LWI values plotted vs the ground temperature T_g. Curves represent the black body emissions with emissivity 1, 0.8, 0.6 and 0.4 from top to bottom respectively.

of the scatter plot of LWI standard deviation calculated over a 20-minute time interval vs LWI itself centred on the same interval. Its application requires the determination of a suitable clear sky LWI limit and associated standard deviation thresholds. For the latter, a value of 0.8 W m^{-2} was chosen according to Town *et al*. (2007), while the monthly longwave thresholds were determined on the basis of the Santa Barbara Discrete Ordinate Radiative Transfer (DISORT) Atmospheric Radiative Transfer (SBDART) code (Richiazzi *et al*. 1998) calculations.

Temperature, pressure and water vapour density monthly mean profiles under clear sky conditions, as defined by Tomasi *et al*. (2010), were used in SBDART calculations. Due to the lack of ozone profile data over Dome C, the standard sub-Arctic winter and summer ozone density profiles were used. The negligible influence of ozone density profiles in evaluating LWI using SBDART does not affect the results given by the scatter plot method, and this approximation does not significantly affect evaluations presented in this paper.

Values of these thresholds from January–December are given in Table I for Dome C. They assume a minimum of 68 W m^{-2} in September, and a maximum of 115 W m^{-2} in December.

The left panels of Fig. 1 shows the scatter plots for January (Fig. 1a) and July (Fig. 1c), which represent typical conditions occurring in summer and winter, respectively. Following Town *et al*. (2007), the bottom-left part of each scatter diagram (quadrant I) is assumed to pertain to clear sky conditions while quadrant IV is assumed to represent overcast conditions and quadrants II and III represent partially cloudy conditions. The right panels of Fig. 1 report the corresponding scatter plot of LWI vs T_g and a series of grey-body curves with emissivities varying between 1.0 (black body) and 0.4. Points with the lower LWI standard deviation are confined between the 0.4–0.6 emissivity range during January (Fig. 1b), while they cover mainly the 0.5–0.7 emissivity range during July (Fig. 1d).

As the LWI is expected to be higher in the presence of clouds than in clear skies, for the same near-surface temperature, the upper limit of such a dataset can be considered to be representative of overcast conditions, while the lower limit pertains to clear skies, in accordance with the scatter plot method shown in the left part of Fig. 1. On the other hand, cloudy-sky cases, for which effective emissivity values greater than unity were observed, correspond to strong temperature inversions in conjunction with the presence of low-level stratus clouds, as shown by König-Langlo & Augstein (1994).

Using this method, the complete Dome C dataset was evaluated. The frequencies of clear sky varied from 35% in May, the cloudiest period, to 70% in February. Table I shows the monthly mean and standard deviations σ_{LWI} of LWI.

https://doi.org/10.1017/S0954102013000096 Published online by Cambridge University Press

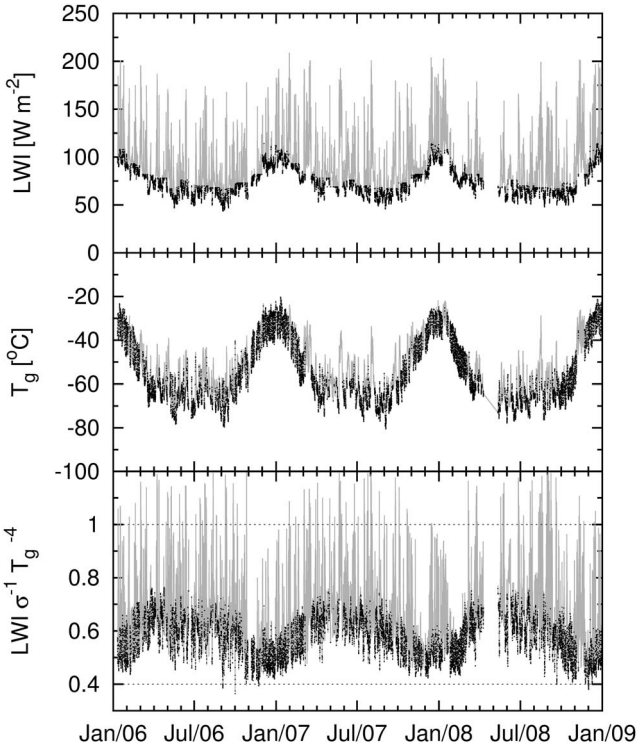

Fig. 2. Dome C data. Upper part: time series of the longwave irradiance (LWI). Middle part: time series of ground temperature T_g. Lower part: time series of the equivalent black-body emissivity $\varepsilon_g = \mathrm{LWI}\sigma^{-1}\mathrm{T_g}^{-4}$. Grey lines represent all-sky conditions, and black dots represent clear sky cases detected with the scatter plot method described in the text.

Figure 2 shows the time series of LWI, T_g and the effective emissivity ε_g calculated for inversion of Eq. (2) with respect to T_g. Longwave irradiance varies in the range 50–200 W m^{-2}, showing seasonal behaviour in phase with the ground temperature T_g, with minima during colder seasons, and in general related to clear sky conditions identified by the black points. The upper LWI limit decreases by about 100 W m^{-2} considering only clear sky cases (black points). The strong cooling of the air at the ground level, expected to be more frequent during clear sky conditions, can be better observed during winter when the clear sky cases occupy the lower limit of the curve in the central graph of Fig. 2. By contrast, during summer, when the surface warms due to the interaction with solar radiation, clear sky cases span the entire temperature interval. The effective emissivity calculated from the previous time series confirms the results observed in Fig. 1b & d for January and July, giving a well defined overview of the range spanned in all-sky (0.4–1.1) and clear sky (0.4–0.7) situations. For clear sky cases the seasonal oscillation is counter-phased to LWI and T_g, indicating that the surface temperature is not representative of the overall thermal conditions of the boundary layer. In fact, the extremely low temperatures reached during winter due to a radiative cooling of the surface are not matched by a corresponding decrease of the LWI. Therefore, if T_g is used to describe LWI through Eq. (1), a variable effective emissivity is required.

Radiosonde data and surface inversions

Radiosondes are routinely launched at Dome C every day at 12h00 UTC (20h00 LT), employing Vaisala radiosondes, model RS92. The measurements performed from January 2006–December 2008 were examined in order to study the behaviour of the thermal inversion structure.

Each radiosonde measurement provides values of the thermodynamic parameters (pressure, air temperature, relative humidity) along with other supplementary data such as wind speed and direction, up to an altitude of about 20 km with a resolution of about 8–12 m in altitude. Radiosonde temperature data can be affected by two kinds of errors, the first arising mainly from solar heating and heat exchange between the radiosonde thermocap sensor

Table II. Values of radio sounding statistical parameters evaluated at Dome C in the three-year period from 1 January 2006–31 December 2008: first row gives the number of radiosonde launches, second row the percentage of temperature profiles with inversion in the ground layer. Parameters T_g, σ_{Tg}, T_m, σ_{Tm}, T_{400} and σ_{T400} are the monthly means and standard deviations of ground, inversion and 400 m temperature, respectively; ΔT is the difference T_g - T_m, H is the mean value of the inversion layer height. All values are valid for the time of the radiosonde (20h00 local time), and, for January and December, they have been calculated for the inversion cases only.

	Jan	Feb	Mar	Apr	May	Jun	Jul	Aug	Sep	Oct	Nov	Dec
n	71	67	65	66	70	73	62	60	51	55	62	62
%	51	99	100	100	100	100	100	100	100	100	98	60
T_g (K)	241.4	229.7	218.9	212.3	211.2	209.4	210.4	211.8	210.7	216.1	233.7	241.4
σ_{Tg} (K)	1.9	5.9	7.8	5.7	8.2	7.5	6.7	8.5	8.2	4.9	5.6	2.2
T_m (K)	243.7	239.7	238.8	237.5	235.9	235.1	235.2	235.2	234.1	234.2	241	242.8
σ_{Tm} (K)	2.1	2.9	3.9	3.3	4.5	3.8	3.3	4.2	4.2	2.4	3.9	2.2
T_{400} (K)	242.8	239.3	238.2	236.9	235.4	234.6	234.9	234.7	233.6	233.8	240.3	241.6
σ_{T400} (K)	2.8	3	3.6	3.3	4.4	3.6	3.3	4.2	4.2	2.4	3.8	2.3
ΔT (K)	2.3	10	19.9	25.2	24.7	25.8	24.8	23.4	23.4	18.1	7.4	1.4
H (m)	188	439	516	547	440	476	417	428	416	422	366	85
$(T_{400}/T_g)^4$	1	1.2	1.4	1.6	1.6	1.6	1.6	1.5	1.5	1.4	1.1	1

https://doi.org/10.1017/S0954102013000096 Published online by Cambridge University Press

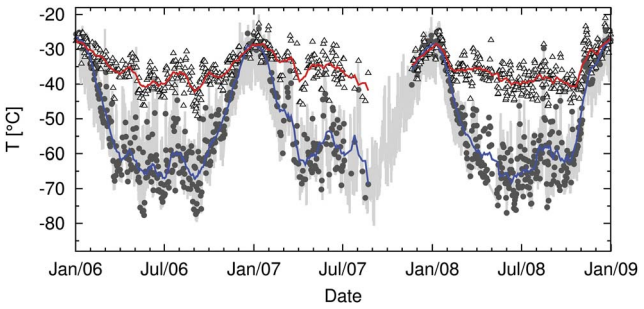

Fig. 3. Time series of ground temperature T_g (circles) and temperature at 400 m T_{400} (triangles) measured by the radiosondes at 20h00 local time. Vertical grey bars represent the daily surface temperature variations measured by the automatic weather station. Red and blue lines represent running averages of T_{400} and T_g calculated over a box of 30 days, respectively.

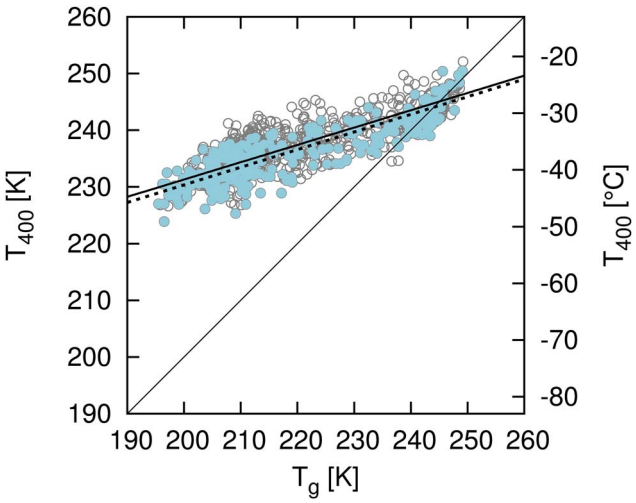

Fig. 4. Scatter plot of temperature at 400 m T_{400} vs ground temperature T_g for all radio sounding performed at 20h00 local time available for the entire period (2006–08) at Dome C. Grey points refer to all sky conditions and cyan points to clear sky. Reported linear fits have been evaluated only for thermal inversion cases. Filled line refers to Dome C clear sky points, dashed line to Dome C all-sky.

and the surrounding air, the second due to the time lag of sensor response. The heat exchange errors were corrected following the standard procedure provided by Vaisala, according to Luers (1997), while the time lag error for RS92 radiosondes was negligible, and hence, no correction was made to the raw temperature data.

Using Dome C radiosonde data, we found that the maximum temperature in the lower troposphere during winter is reached at a height of about 400 m. During January and December the inversion is weak or is replaced by almost isothermal conditions. Moreover, Aristidi *et al*. (2005) and Hudson & Brandt (2005, their fig. 22) highlighted the fact that the temperature inversion extends usually up to 150 m and temperature profile above 150 m is isothermal with height and stable (within *c*. 2 K) during summer days.

Ricaud *et al*. (2012) showed, based upon microwave radiometer measurements carried out at Dome C, that there is a weak diurnal variation of temperature (ΔT) above 150 m. The effect of this variation on LWI in T is <1 W m^{-2}, and so can be neglected.

Based on these observations, we have adopted T_{400} as a good approximation of T_m. A similar assumption was adopted by Yamanouchi & Kawaguchi (1984), who studied longwave emissions under surface inversions at Mizuho (Antarctica), utilizing the temperature measured at 300 m, the typical inversion level at that site.

Table II reports the values of some statistical parameters characterizing the temperature profiles, obtained on a monthly basis, using the Dome C radio soundings. For January and December the values were calculated only for the inversion cases. From February–November the temperature inversion is always present, while the frequency of inversion cases is smallest in December (50%) and January (60%). During these two months the inversion strength ΔT, defined as T_{400} - T_g, assumes minimum values, i.e. about 2 K on average, when the temperature inversion is frequently replaced by isothermal conditions. From March–October ΔT assumes values around 20 K or higher and is quite stable during the period. This atmospheric temporal stability is an important feature of the winter in the high Antarctic Plateau (Phillpot & Zillman 1970). The seasonal differences between winter and summer conditions are similar to those reported by Hudson & Brandt (2005) for South Pole. This behaviour is mainly due to the effect of the solar radiation on the snow surface, which causes convective activity due to surface heating (Argentini *et al*. 2005). Table II clearly shows that monthly averages of T_m and T_{400} are consistent within their standard deviations. These standard deviations are generally lower than that of T_g, except for January and December when the inversion is much weaker, indicating that the maximum temperature is more stable than the ground temperature throughout the year. Figure 3 shows the time series of T_{400} and T_g. The ground temperature varies seasonally by about 60°C from -80°C to -20°C, while T_{400} varies by only 30°C, from -45°C in winter to -15°C in summer.

Figure 4 shows the plot of T_{400} vs T_g, as obtained from both all-sky and clear sky radiosonde data. Clear sky conditions are selected using the results of the scatter plot method, obtained within a period of ± 1h around the nominal launch time of 20h00 LT. Since the scatter plot method flags cloudy/clear each minute, the radiosonde is considered to be performed for clear sky conditions if at least 90% of the flight period was detected as clear. Figure 4 shows that the best fit regression line, calculated only for inversion cases, does not change appreciably between clear and cloudy contaminated radiosonde measurements. This confirms that the presence of clouds of a low optical depth on the Antarctic Plateau does not

https://doi.org/10.1017/S0954102013000096 Published online by Cambridge University Press

significantly affect the establishment of a thermal inversion in the boundary layer caused by surface cooling. The linear best fit for clear sky cases is given by:

$$T_{400} = 168 + 0.31T_g, \tag{3}$$

with temperatures expressed in Kelvin and a regression coefficient of $r^2 = 0.86$.

In terms of inversion strength ΔT defined as the difference between T_{400} and T_g, Eq. (3) can be rewritten as $\Delta T = 168 - 0.69T_g$. Here, the slope coefficient we found is about 10% higher than that indicated by Connolley (1996) for the interior of the continent, using monthly averages of T_m and T_g measured at Vostok and South Pole.

Figures 3 & 4 also show that, in the higher temperature range, some values of T_{400} are very close to T_g, indicating cases without inversion. For these conditions, observed only during January and December as shown in Table II, the mean ground temperature value, 246.1 K in January and 245.8 K in December, is comparable to the mean value of the measured T_{400}, 246.2 K and 245.0 K, respectively for January and December, highlighting an isothermal-like behaviour of the lower troposphere in the absence of an inversion. Nearly isothermal conditions in the lowest kilometre of the troposphere were also reported by Hudson & Brandt (2005) during summer months at South Pole. Applying Eq. (3) to these cases leads to mean value of the computed T_{400} of 244.3 K in January and 244.2 K in December, both lower than observed. Hence, without thermal-based inversion conditions, the proxy temperature T_{400} is considered equal to the ground temperature and not calculated using Eq. (3). On average, it is possible to define a temperature threshold of about 244 K, above which inversion never occurs, given by the intersection of Eq. (3) with the condition $T_{400} = T_g$.

Considering both the cases of inversion and its absence, the relationship providing T_{400} as a function of T_g becomes:

$$T_{400} = f(T_g) = \begin{cases} 168 + 0.31T_g & T_g \leq 244K \\ T_g & T_g > 244K. \end{cases} \tag{4}$$

Ground temperature diurnal cycle

Equation (4) is valid only for the time interval during which each radio sounding is performed at Concordia Station, i.e. at 12h00 UTC (20h00 LT). The use of Eq. (4) at a different time t of the day should induce a certain inaccuracy in evaluating $T_{400}(t)$, because of the strong variations of $T_g(t)$ throughout a summer day, from a morning minimum to a maximum in the early afternoon, closely related to the solar zenith angle cycle. In fact, Eq. (4) attributes approximately one third of the T_g daily variation amplitude to T_{400}, in case of inversion while, without inversion, T_{400} and T_g assume the same daily variation amplitude. As pointed out in the previous section, Hudson & Brandt (2005), Aristidi *et al.* (2005) and Ricaud *et al.* (2012) showed that diurnal variation is negligible at levels over 150 m. Hence, $T_{400}(t)$ during the day can be considered equal to the temperature at 400 m recorded by the radiosonde at 20h00 LT, i.e.

$$T_{400}(t) \approx T_{400}^{RDS} \approx f(T_g^{RDS}), \tag{5}$$

where the form of function f has been given in Eq. (4) and T_g^{RDS} is the ground level temperature measured during radiosonde flight.

There is also a variability in the temperature that is not linked to the incoming solar radiation, especially during winter, which is instead due to the approach of cyclones to Antarctica from lower latitudes (Enomoto *et al.* 1998) and to interplanetary magnetic field variation (Troschiev *et al.* 2008). In all cases such temperature variations are associated with a cloud layer formation at heights of 6–8 km (Troshichev *et al.* 2008, page 1297), and they were not considered here since the parameterization given in this paper is for the clear sky emissivity.

Figure 5 reports the monthly mean T_g daily evolutions. In the left part, the months characterized by presence of sun are reported, while in the right part, data are plotted for months without sunshine relevant effects. The T_g diurnal variation can be referred, following a method similar to that of Dürr & Philipona (2004), to the daily average ground temperature $\overline{T_g}$, through a simple sinusoidal form with a 24-hour period, appropriate amplitude A_d, angular frequency $\omega_d = 2\pi / 24$ and a phase φ_d, as follows:

$$T_g(t) = \overline{T_g} + A_d \cos(\omega_d t + \varphi_d), \tag{6}$$

where the time t is expressed in LT hours.

As shown in Fig. 5, amplitude A_d can be assumed equal to 6 K for the summer months November–February, 4 K for March and October, 2 K for transitional months April and September (left part of Fig. 5), and zero for the other winter

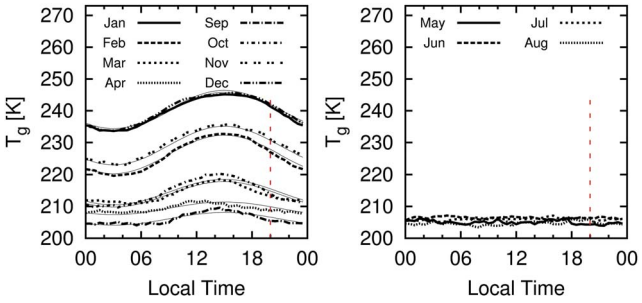

Fig. 5. Left: Dome C data. Monthly mean daily behaviour of the ground temperature T_g for months from September–April. Right: same values plotted for polar night months (June and July) and last/first sunrise month (May and August). The vertical dashed lines correspond to the radiosonde launch time (20h00 local time), the filled lines reproduce Eq. (6) with phase $\varphi_d = 3\pi/4$ and amplitude $A_d = 6$ K from November–February, 4 K for March and October, 2 K for April and September and set to zero for the months reported in the right part of the figure.

https://doi.org/10.1017/S0954102013000096 Published online by Cambridge University Press

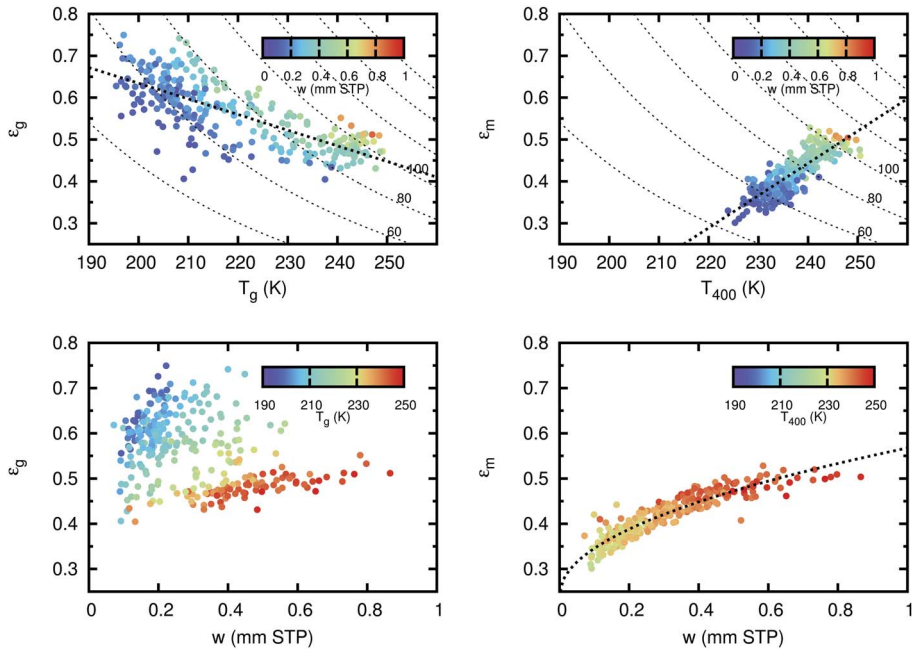

Fig. 6. Left: clear sky effective emissivity, $\varepsilon_g = \mathrm{LWI}\sigma^{-1}\mathrm{T_g}^{-4}$ plotted vs T_g (upper part) and vs vertical water content w obtained from Dome C radiosondes (lower part). Right: clear sky effective emissivity, $\varepsilon_m = \mathrm{LWI}\sigma^{-1}\mathrm{T}_{400}^{-4}$, plotted vs T_{400} (upper part) and w (lower part). Regression lines for $\varepsilon_g(T_g)$, $\varepsilon_m(T_{400})$ and $\varepsilon_m(w)$ are reported. In the lower part points colour represent T_g (left) and T_{400} (right), while in the upper plots, the colour scale represents w. The isolines of longwave irradiance (LWI) are also reported in steps of 20 W m^{-2} in the upper part of the figure.

months (right part of Fig. 5) when there is no sun and, hence, daily variation is absent. The phase φ_d was evaluated to be well represented by 3/4π on average, a value that shifts the cosine function nine hours early. This phase value provides good fits in January, February, November and December, when the diurnal cycle is more evident. The assumption of the same value over the whole year does not significantly affect the results because the amplitude becomes gradually lower moving towards winter.

From Eq. (6), the temperature T_g^{RDS} at radiosonde launching time (20h00 LT), can be evaluated in terms of the following equation:

$$T_g^{RDS} = T_g(t) - A_d\left[\cos\left(\omega_d t + \phi_d\right) - \cos\left(\omega_d t^{RDS} + \phi_d\right)\right]. \tag{7}$$

Combining Eqs (5) & (7), T_{400} for clear sky conditions can be evaluated during the whole day using the following equation:

$$T_{400}(t) = f\left(T_g(t) - A_d\left[\cos\left(\omega_d t + \phi_d\right) - \cos\left(\omega_d t^{RDS} + \phi_d\right)\right]\right), \tag{8}$$

where the function f has been defined in Eq. (4).

Parameterization of clear sky emissivity

As previously discussed, the clear sky longwave flux and emissivity can be expressed in terms of appropriate temperature values, which should be chosen to realistically represent the thermal conditions of the boundary layer. Usually the ground temperature T_g is adopted. However, we have used T_{400}, taking into account that T_{400} and T_g are related by Eq. (8).

Effective emissivity was evaluated by inverting Eq. (2), using hourly averages of LWI corresponding to radiosonde launching, and both T_g and T_{400} as reference temperatures. The left panels of Fig. 6 show the emissivity calculated with respect to the ground temperature ($\varepsilon_g = \mathrm{LWI}/\sigma T_g^4$) vs T_g itself (upper) and vs precipitable water content w as obtained from radiosonde (lower), while the right panels show emissivity calculated using T_{400} ($\varepsilon_m = \mathrm{LWI}/\sigma T_{400}^4$) vs T_{400} (upper) and w (lower). It is evident that effective emissivity is better correlated with temperature and w, when it is calculated with respect to T_{400} rather than T_g. Furthermore, ε_g results to decrease with T_g showing an unrealistic behaviour. In fact, as temperature increases the saturation vapour pressure increases and hence, emissivity is expected to increase.

The regression line reported in the right part of Fig. 6, relating to T_{400}, is

$$\varepsilon_m = -1.41 + 0.0077 T_{400}, \tag{9}$$

which shows an increase in the emissivity with increasing reference temperature, as expected. Assuming a square root dependence of the emissivity on water vapour content, experimental data can be approximated by $\varepsilon_m = 0.24 + 0.32\sqrt{w}$ (w in g cm^{-2}) with a regression coefficient $r^2 = 0.8$. By contrast, ε_g does not show an evident correlation with w.

These considerations confirm that, in the presence of a temperature inversion, the use of T_{400} is more appropriate than T_g, in describing the emission properties of the atmosphere. In order to evaluate the emissivity as a function of ground based measurements, T_{400} was preferred to w since it is easily related with T_g and because measuring RH using standard procedures is quite problematic in such cold and

https://doi.org/10.1017/S0954102013000096 Published online by Cambridge University Press

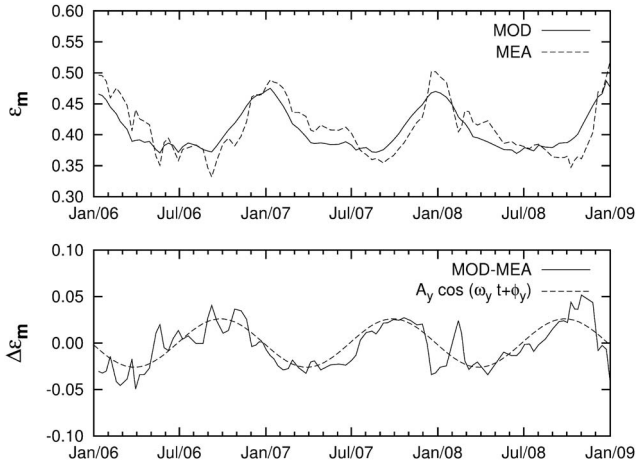

Fig. 7. Upper part: emissivity ε_m modelled using Eq. (11) (MOD) and obtained from measurement as $LWI\sigma^{-1}T_m^{-4}$ (MEA) for the three-year Dome C dataset. Lower part: difference between modelled and measured emissivity with the corresponding best fit given in Eq. (10).

dry environments. Furthermore, there is a linear relationship between w and T_{400} with a correlation coefficient $r^2 = 0.8$ (not shown), indicating that T_{400} itself contains information on the precipitable water content, since the saturation vapour pressure increases with air temperature.

Since both LWI and T_{400} show little diurnal variability on clear sky days, Eq. (9) can be assumed to be valid for the whole day.

Using Eqs (8) & (9), we compare the modelled emissivity with field measurements. The upper panel of Fig. 7 shows the time variability of the modelled and measured values of ε_m, and the lower panel shows their difference. Figure 7 highlights the existence of an annual cycle in the difference between modelled and measured values, presumably due to the variation of water vapour content, inversion strength, and other effects neglected in Eq. (9). In order to take this feature into account, the following time-dependent sinusoidal correction for the emissivity, with a one-year (365.25 days) period, was added:

$$\Delta\varepsilon_m = \varepsilon_m^{MOD} - \varepsilon_m^{MEA} = A_y \cos\left(\omega_y d + \varphi_y\right), \qquad (10)$$

where d is the day of the year, $A_y = 0.0261$, $\omega_y = 2\pi / 365.25$ and $\varphi_y = 1.66$. Such a phase value anticipates the maximum overestimation by 115 days with respect to the end of the year, placing it at the beginning of September. Similarly, the maximum underestimation was found in March, corresponding to a delay of a couple of months with respect to the warmest and moistest period of the year (December–January).

Inserting this time-dependent correction into Eq. (9), the following updated equation was obtained:

$$\varepsilon_m = -1.41 + 0.0077T_{400} - A_y \cos\left(\omega_y d + \varphi_y\right). \qquad (11)$$

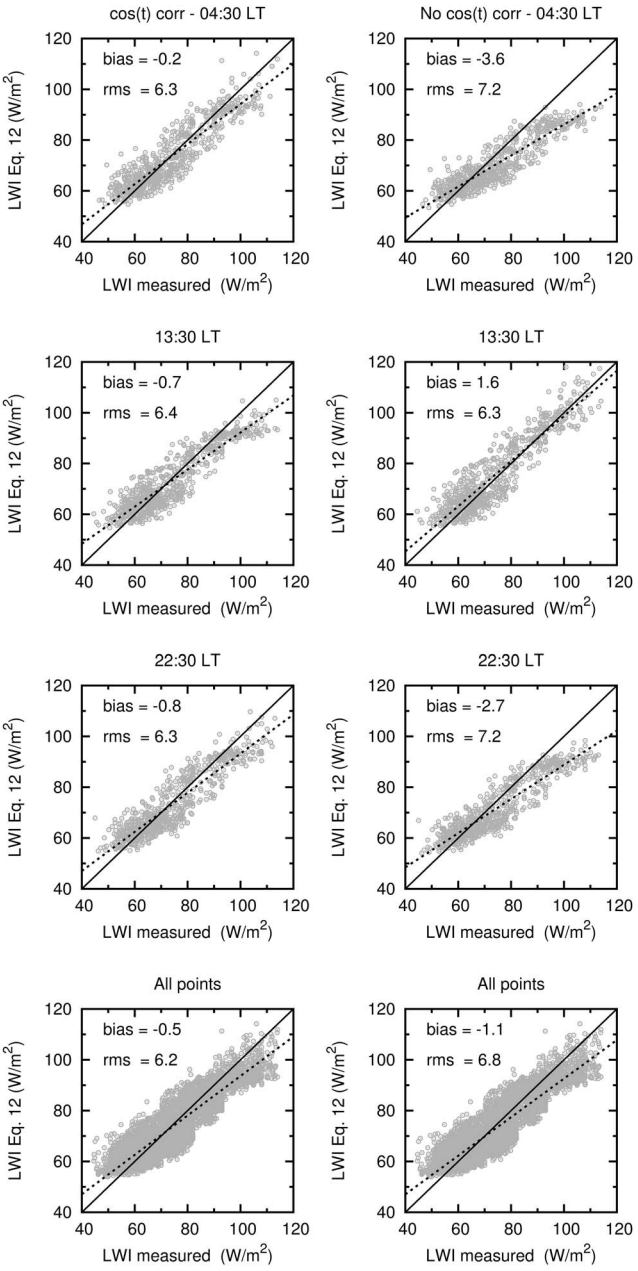

Fig. 8. Scatter plot of hourly averaged longwave irradiance (LWI) modelled using Eq. (12) and measured LWI for the whole three-year Dome C dataset at different local times. Left: Calculation of LWI with the time dependency of ground temperature of Eq. (8). Right: modelled LWI are calculated without the cosine correction. In all the plots the filled line represents the equation y = x and the dotted line the linear correlation. Bias, evaluated as the difference between modelled and measured values, and the root mean square (RMS) value, are also reported for each scatter plot.

Equation (11) gives the emissivity with respect to T_{400}. Using Eq. (2), we can calculate LWI with $\varepsilon_m\sigma T_{400}^4$ as long as $\varepsilon_g\sigma T_g^4$, the latter expression being comparable with most

https://doi.org/10.1017/S0954102013000096 Published online by Cambridge University Press

Table III. Description of the models of ε_{eff} used as concurrent for testing the parameterization developed in this study, including regions in which they were parameterized and air temperature range, when available.

Model	ε_{eff}	Experimental site	T_{min}/T_{max}(°C)
Swinbank 1963	$9.365 \times 10^{-6}\ T^2$	Australia, Indian Ocean, England and France	+2/+29
Idso & Jackson 1981	$1–0.261\ e^{(-7.77E-4(273\ -T)\^2)}$	Alaska, Arizona, Australia	-29/+37
Ohmura 1982	$8.733 \times 10^{-3}\ T^{0.788}$	Axel Heiberg Island (Canadian Arctic Archipelago)	Not available
Guest 1998	$1–85.6/\sigma T^4$	Weddell Sea (Antarctica)	-27/0

parameterizations. The relation between two forms of emissivity, $\varepsilon_g = \varepsilon_m \left(T_{400} / T_g\right)^4$, allows to express LWI as a function of T_g:

$$LWI = \varepsilon_m \left(\frac{T_{400}}{T_g}\right)^4 \sigma T_g^4, \tag{12}$$

with T_{400} evaluated using Eq. (8) and ε_m using Eq. (11).

Application of the methodology to South Pole data

South Pole, located on the Antarctic Plateau (89.98°S, 24.80°W, 2800 m above mean sea level), is a good site for testing the methodology presented in this paper for the calculation of LWI. South Pole has a similar atmospheric thermal structure to that observed at Dome C. Strong surface thermal inversions occur during winter, with mean strengths of 20–25 K, while the inversions are weaker or absent during summer (Hudson & Brandt 2005).

The relationship between T_{400} and T_g is site-dependent, and needs to be reformulated for South Pole. First of all the daily cycle is not present, South Pole being situated at nearly 90°S, and T_g can be considered constant during the clear sky days. Therefore the relationship between T_{400} and T_g does not contain the time dependence term of Eq. (8).

Using radiosonde data obtained from the Wyoming University website (http://weather.uwyo.edu/upperair/sounding.html, accessed March 2010), a linear relationship between T_{400} and T_g, and the threshold temperature over which inversion should not occur were recalculated for South Pole, i.e.

$$T_{400} = f(T_g) = \begin{cases} 161 + 0.35 T_g & T_g \le 248K \\ T_g & T_g > 248K \end{cases}, \tag{13}$$

with regression coefficient $r^2 = 0.82$.

Comparing coefficients of Eqs (4) & (13), the South Pole linear best fit does not differ significantly from that evaluated for Dome C. This confirms the similarity of the thermal structure of the lower troposphere between the two plateau sites. Moreover, the precipitable water content values were found to be similar to those of Dome C, with values that vary from 0.1–0.8 mm at standard temperature and pressure (STP). Due to this similarity, the relation between ε_m and T_{400} can be assumed to be valid for both plateau sites.

Once T_{400} is evaluated using Eq. (13), it is possible to calculate the emissivity at South Pole, making use of Eq. (11), and hence the LWI from Eq. (12).

Results

The summer daily cycle

Figure 8 highlights the significant role of Eq. (8), which introduces the time-dependent cosine factor to correct for

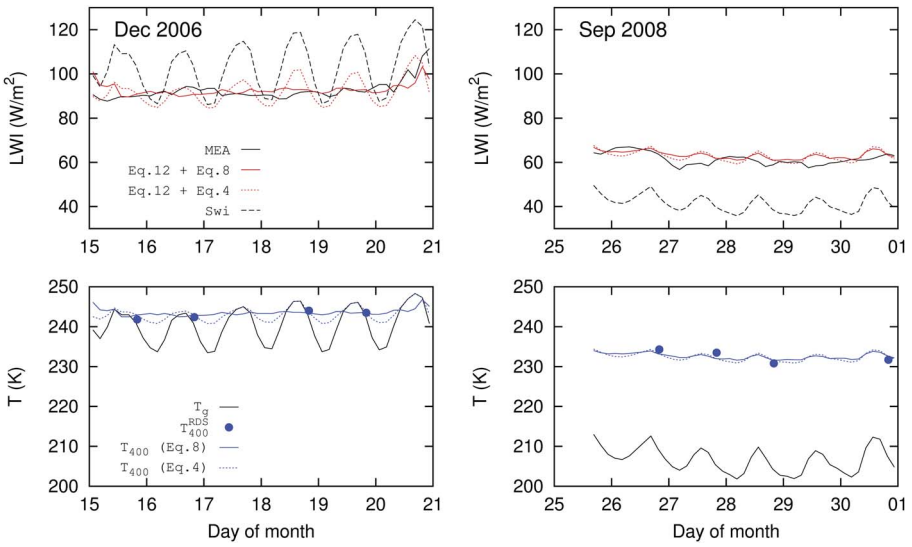

Fig. 9. Dome C data. Upper part: time patterns of measured and calculated longwave irradiance (LWI) using Eq. (12), with (Eq. (8)), and without (Eq. (4)) the daily cosine correction of T_{400}. Longwave irradiance estimated with Swinbank parametric equation (Swi) is also reported. Lower part: measured value of T_g, T_{400} calculated using Eq. (8) and T_{400} calculated using Eq. (4). Blue points refer to the T_{400} measured by radiosonde. Left: summer period of December 2006. Right: same as before but for a colder winter period (September 2008).

https://doi.org/10.1017/S0954102013000096 Published online by Cambridge University Press

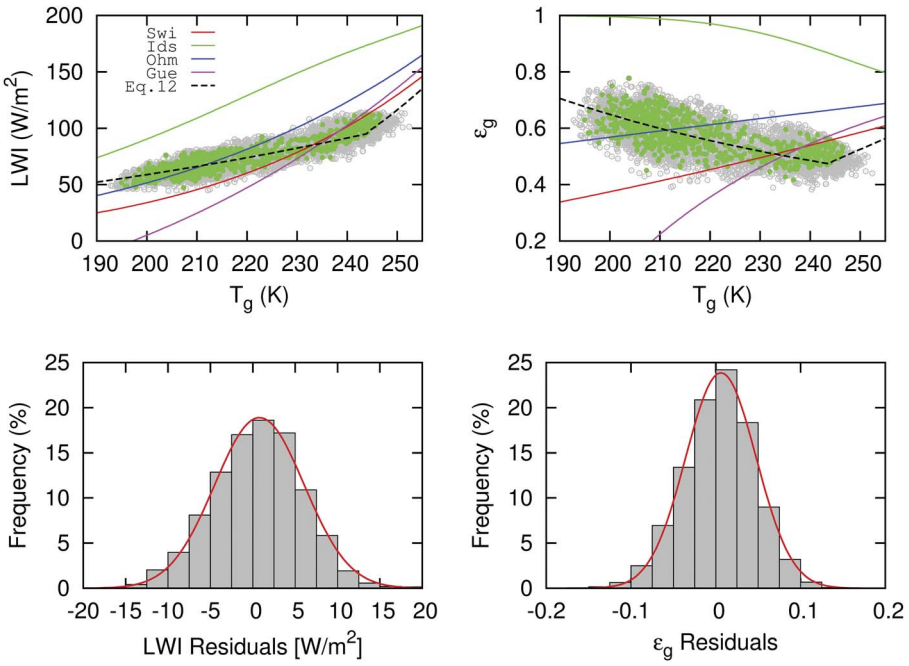

Fig. 10. Dome C data. Upper part: longwave irradiance (LWI) (left) and ε_g (right) plotted vs T_g. Grey and green points show the three-hour and daily averages of measured quantities, respectively. The parameterizations of Swinbank (1963), Idso & Jackson (1969), Ohmura (1982) and Guest (1998), are reported along with Eq. (12) (left) and Eq. (11) (right). Lower part: evaluation of residual, calculated as difference between measured and parameterized values for the three-hour averaged data, for the LWI (left) and ε_g (right), with the best fit Gaussian curve in red.

the daily cycle of T_g and maintains T_{400} constant during a day. The left panels of Fig. 8 show the scatter plot of the modelled vs measured LWI, while the right panels show the scatter plot of the estimates of LWI calculated without the cosine correction vs the field measurements. Data obtained for the overall three-years dataset recorded at night time (04h30 LT), day time (13h30 LT), and evening time (22h30 LT) are reported, as well as for those for the entire day. Without the time-dependent correction, the correlation between estimated and measured LWI varies according to the hours considered, providing better results for the warmer hours of the day (bias equal to 1.6 W m^{-2} and root mean square (RMS) equal to 6.3 W m^{-2} at 13h30 LT), and the worst results during the night hours (bias and RMS equal to -3.6 W m^{-2} and 7.2 W m^{-2}, respectively at 04h30 LT). Using the cosine correction, the correlation does not vary much with time, with RMS values at different times of the day almost equal to 6.3 W m^{-2}, while the bias reaches its minimum at 04h30 LT (-0.2 W m^{-2}) and its maximum at 22h30 LT (-0.8 W m^{-2}). Considering the overall dataset, RMS values for both estimates are similar: 6.2 W m^{-2} with cosine correction and 6.8 W m^{-2} without. However, the bias is lower for the cosine corrected estimation (-0.5 W m^{-2}) than for the estimation without cosine correction (-1.1 W m^{-2}). Thus, the introduction of Eq. (8) provides more accurate forecast of the time pattern of LWI during a sunny day.

Table IV. Bias and root mean square (RMS) values between measured longwave irradiance (LWI) and that obtained with the parameterizations given in Table III, including the present one and the one developed in this study. Calculation has been done for the three-hours running average of the three-years dataset. All values in W m^{-2}.

Study		Jan	Feb	Mar	Apr	May	Jun	Jul	Aug	Sep	Oct	Nov	Dec	Year
This study	bias	-0.1	-1	-5.2	-5.3	0.9	-1.9	0.2	1.2	4.5	5.5	7.6	3.1	0.8
	RMS	4.8	5.6	7	7	4.6	5.4	4.6	4.6	6.3	7.3	8.4	7	6.2
Swinbank 1963	bias	4.4	-9.5	-22.7	-25.3	-21	-23.1	-21.2	-21	-17.1	-11.6	1	8.5	-12.2
	RMS	12.2	14.8	23.7	25.8	21.8	23.8	22	21.7	18.1	14.1	10.1	13.9	18.8
Idso & Jackson 1969	bias	69.2	59.6	42.9	37.8	39.2	38	40	38.9	43.8	54.3	70.3	72.8	51.6
	RMS	69.7	60.7	43.8	38.4	40.1	38.8	40.6	40	44.6	55.3	70.9	73.2	54.1
Ohmura 1982	bias	26.2	12.1	-2.5	-5.8	-2.3	-4.2	-2.3	-2.5	1.7	8.7	22.8	30.2	7.9
	RMS	28.4	16.9	7.7	7.9	7	7.6	7.1	6.2	6.5	12.3	25	32	17.3
Guest 1998	bias	5.2	-17.7	-40.1	-46.3	-77.5	-55.2	-44.8	-50.9	94.1	-28.5	-5.1	9.7	-34.2
	RMS	15	23.6	41.3	46.8	194	110	45.7	87.8	246	30.8	14.7	16.4	96.6

https://doi.org/10.1017/S0954102013000096 Published online by Cambridge University Press

As shown by Guest (1998) and Pirazzini *et al*. (2000), various parametric models have been proposed in the literature for clear sky effective emissivity, based on the analytical forms listed in Table III. All the formulations reflect the summer daily cycle of T_g on LWI. The parameterization given in Eq. (11) depending on T_{400}, does not show any daily cycle in agreement with measured LWI, because of the introduction of the cosine correction in the relation between T_g and T_m.

The upper panels of Fig. 9 show the time patterns for a summer (January) and a winter (September) period, characterized by the sun's presence, of the following quantities: i) measured LWI; ii) LWI calculated using Eq. (12), where T_{400} is calculated with cosine correction, Eq. (8); iii) LWI calculated using Eq. (12), where T_{400} is calculated without cosine correction, Eq. (4); and iv) LWI calculated using the Swinbank (1963) formula.

In the lower panels of Fig. 9 the values of T_{400}, calculated using Eqs (8) & (4), and of T_g are plotted for the same periods.

The LWI calculated using the Swinbank (1963) formula shows, especially during summer, a daily variation of about 25 W m^{-2} following the ground temperature variation, leading to an error that could be as high as 20 W m^{-2}. The LWI calculated with the parameterization of Eq. (12) without the cosine correction also shows a daily variation, but with a smaller amplitude of about 15 W m^{-2}, being related to the variation of T_{400} estimated with Eq. (4) and shown in the bottom part of Fig. 9. Taking the cosine correction of Eq. (8) into account in Eq. (12), the estimated values of LWI are not affected by the temperature daily cycle, and better approximate the measured values of LWI. These features are stronger in January, when the solar zenith angle variation is more pronounced, causing a more evident ground temperature daily cycle.

Comparison with other parameterizations

Figure 10 shows clear sky values of LWI and ε_g evaluated with the parameterizations given in Table III together with those obtained in this study - Eq. (12) - over the whole temperature range observed at Dome C. The dark grey points provide the three-hour running average values of LWI and ε_g vs T_g under clear sky conditions, while green points refer to their daily averages. Figure 10 clearly shows how the Idso & Jackson (1969) parameterization leads to overestimated values of LWI over the whole temperature range. The curve obtained by Ohmura (1982) fits the LWI measurements better at low temperatures ($T_g < 230$ K) mainly observed during winter time, than at higher temperature, where it produces significantly overestimated values. Swinbank (1963) and Guest (1998) formulas give better results within the higher temperature range, but they significantly underestimate values at low temperatures.

These remarks are summarized in Table IV, where bias and RMS values, evaluated as difference between estimated and measured values of LWI, are reported for each month and for the whole three-year dataset using three-hour average data. Bias and RMS evaluated for Eq. (12) are almost constant throughout the year, emphasizing that the correlation does not depend much on the temperature range. Taking the complete dataset into consideration, the parameterizations developed in the present study provide the lowest bias and RMS values, indicating the best agreement with measurements.

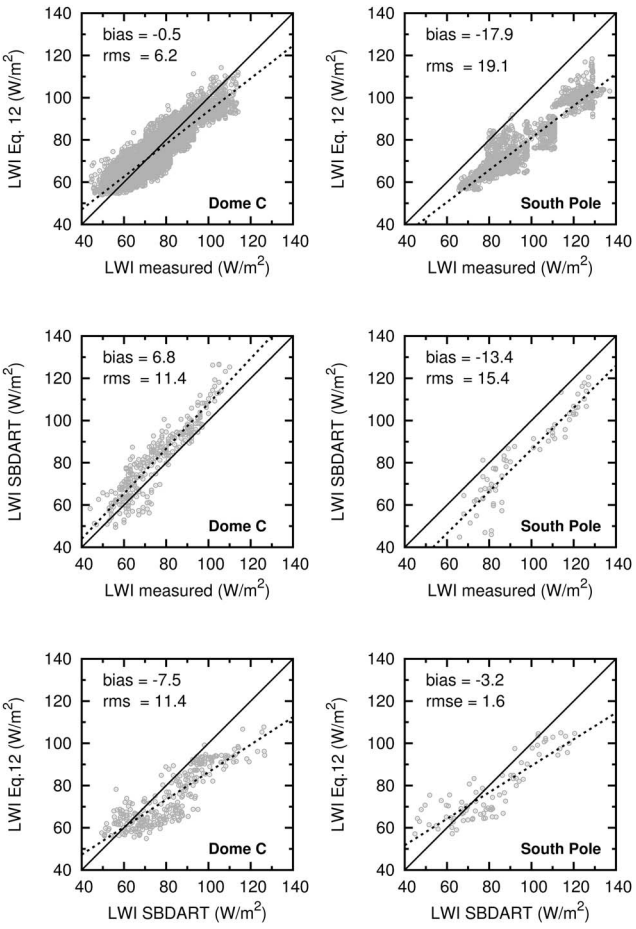

Fig. 11. Comparison, for both Dome C (left) and South Pole (right), between measured longwave irradiance (LWI) and LWI calculated from the parametric model given in this work (upper part), Santa Barbara Discrete Ordinate Radiative Transfer (DISORT) Atmospheric Radiative Transfer (SBDART) calculation (middle part). Lower part presents comparison between SBDART calculation and present parameterization. In every plot the filled line refers to the equation y = x and the dotted line to the linear correlation. Bias and root mean square (RMS), calculated in W m^{-2}, are also reported.

The right panels of Fig. 10 show the same comparison but in terms of ε_g. All parametric formulations given in Table III predict ε_g to monotonically increase with T_g for the whole temperature range, with the exception of the Idso & Jackson (1969) formula, which instead provides very high

https://doi.org/10.1017/S0954102013000096 Published online by Cambridge University Press

emissivity values that decrease with increasing T_g. Differently, the parametric equation given in Eq. (11) shows two different emissivity domains due to the piecewise function defined in Eq. (4) and included in Eq. (11). At temperatures lower than 244 K, i.e. for surface based thermal inversion, the emissivity decreases as long as T_g increases, while, for temperatures above 244 K, without inversion, it increases linearly with T_g, maintaining a good fitting with observations. Similar features of emissivity were also found by Niemela (2001, their fig. 3), when studying LWI under strong inversion conditions at the Arctic site of Sodankylä (Finland, 67°22'N, 26°39'E). As previously discussed, a negative slope of emissivity is unexpected, unless a poorly representative temperature of the thermal condition of the atmosphere is used in Eq. (2). In fact, using a $T_g << T_m$ implies a forced lowering of simulated LWI, which must be compensated by a high emissivity value ε_g (as shown in Fig. 2). It is obtained by multiplying the most representative ε_m by the $(T_m/T_g)^4$ factor, which accounts the strength of the inversion (Table IV).

The lower panels of Fig. 10 report the residual evaluated as the difference between measurements and values obtained using the parameterization given in this study, for both LWI and ε_g. These residuals are normally distributed, and the fitted Gaussian curve shows a mean value of 0.6 W m^{-2} with a standard deviation of 6.5 W m^{-2} for LWI, while for ε_g the mean value is -0.004 and its variance is 0.05.

Comparison with a radiative transfer model

Figure 11 shows, for both Dome C and South Pole, the comparison between: i) LWI calculated through Eq. (12) and measured LWI, ii) SBDART calculations of LWI and measurements of LWI, and iii) SBDART calculations of LWI and LWI modelled with the parameterization given in the present study. The two latter plots are limited to the radio sounding time, due to the needs of SBDART evaluations. Longwave irradiance for South Pole, obtained from the BSRN website, was measured using a Precision Infrared Radiometer (PIR) manufactured by Eppley.

For Dome C, the values of LWI obtained using Eq. (12) are, on average, underestimated for high temperatures and overestimated for low temperatures, with respect to the measured values. The agreement between measured and estimated values is, however, quite good, the bias and RMS being -0.5 W m^{-2} and 6.2 W m^{-2}, respectively.

The SBDART calculation reproduces the measured values of LWI (bias = -7.5 W m^{-2} and RMS = 1.0 W m^{-2}) with good approximation, although in the high temperature range it slightly underestimates the measured values. The comparison between the two estimations of LWI is reported in the bottom-left part of Fig. 11, which shows a good agreement even if, in general, a weak underestimation of the values calculated with Eq. (12) is evident.

For South Pole, the right panels of Fig. 11 show that the measured LWI values are always higher than the estimated LWI ones obtained by both SBDART calculations (bias = -13.4 W m^{-2} and RMS = 15.4 W m^{-2}) and Eq. (11) procedures (bias = -15.7 W m^{-2} and RMS = 16.3 W m^{-2}). The comparison between SBDART calculations and the present parameterization values indicates a substantial agreement, the bias being equal to -3.2 W m^{-2} and the RMS to 1.6 W m^{-2}.

Conclusions

Surface-based atmospheric thermal inversions are typical of the Antarctic Plateau. In the presence of inversions, parameterizations of emissivity with respect to ground measurements of temperature and/or water vapour are likely to be in error. This observation prompted our attempt to define the clear sky emissivity ε_m, calculated by dividing clear sky LWI values by σT_m^4. The commonly used effective emissivity ε_g can be obtained by multiplying ε_m by the factor $(T_m/T_g)^4$, which takes into account the surface thermal inversion. Finding a relationship between ε_m and T_m, and between T_m and T_g, allows us to estimate the emissivity, and then the LWI, with easily available ground temperature measurements.

With the aim of obtaining a parameterization of LWI that could be applied to the high Antarctic Plateau, the thermal structure of the lower troposphere has been studied at two plateau sites: Dome C and South Pole. Radiosonde measurements from these two stations during 2006–08 indicate that the atmosphere has strong surface inversion conditions during most of the year, with more evident features during winter months. In the presence of this thermal inversion, T_m is well represented by the temperature at 400 m above the surface (T_{400}), such altitude representing the mean height of the inversion. It is related to ground temperature T_g by a linear equation, which is very similar for the two sites. In the few cases of absence of inversion, the temperature profile is nearly isothermal, so the maximum, ground and 400 m temperatures can be considered to be the same. Hence, for the definition of ε_m the proxy temperature T_{400}, calculated in terms of T_g by Eq. (4) for Dome C and Eq. (13) for South Pole, was chosen. For the lower latitude site of Dome C, an evident ground temperature daily cycle is observed during summer months, which can be reliably represented by using a time dependent cosine function, added to the relationship between T_{400} and T_g in order to maintain T_{400} constant throughout the day.

Analysing the BSRN and radiosonde datasets, a linear relationship has been found between the measured ε_m and T_{400}. Combining these two relations produced an empirical parameterization of ε_g in terms of T_g, as commonly adopted in many existing models (Eq. 12).

The parameterization given in this study shows two different behaviours of the emissivity, which decreases with increasing ground temperature when a surface based inversion is present, and increases linearly with ground temperature without inversion, reaching the minimum

https://doi.org/10.1017/S0954102013000096 Published online by Cambridge University Press

value at ground temperature close to -30°C (244 K), which is the temperature above which inversions are not expected to occur. The high values of emissivity ε_g found at low temperatures are due to the inversion, the strength of which is contained in the term $(T_{400}/T_g)^4$ of the parametric equation. This term is equal to one in the absence of inversion and increases at colder ground temperature, when the inversion strength is higher.

With the present study, the importance of surface-based temperature inversion in the evaluation of the atmospheric thermal emission and, thus, in the radiation budget, has been highlighted. We have shown that, for a better estimation of the atmospheric emissivity, it is preferable to refer to the inversion temperature than to ground temperature. The parameterization developed in this study fits the measured data better than other parameterizations based directly on ground measurements only.

Improvements to this parametric equation can be obtained by further investigations of the evolution of the temperature up to 400 m. Useful information could be obtained from continuous measurements of temperature at different heights from the surface up to the first kilometre of atmosphere by using tethered balloons.

The daily cosine correction of temperature T_{400} has been evaluated only for Dome C, and is obviously specific to that site. Its phase and the amplitude should be related to the variation of ground temperature with solar irradiation.

In order to apply the methodology to the whole Antarctic Plateau, a relationship between latitude and the parameters of such a correction should be investigated. Currently, the difficulty of finding complete datasets from other plateau stations makes such an investigation very hard to accomplish.

Acknowledgements

This research was supported by the Programma Nazionale di Ricerche in Antartide (PNRA) and developed as a Subproject 2004/2.04 "Implementation of the BSRN station at Dome Concordia". Meteorological and radiosonde data used in this study were obtained from the "RMO - Osservatorio Climatologico" of the Programma Nazionale di Ricerche in Antartide (PNRA) (http://www.climantartide.it, accessed March 2010). The constructive comments of the reviewers are gratefully acknowledged.

References

Ångström, A. 1918. A study of the radiation of the atmosphere. *Smithsonian Miscellaneous Collection*, **65**, 159–161.

Argentini, S., Viola, A., Sempreviva, A.M. & Petenko, I. 2005. Summer boundary-layer height at the plateau site of Dome C, Antarctica. *Boundary Layer Meteorology*, **115**, 409–422.

Aristidi, E., Agabi, K., Fossat, E., Vernirn, J., Travouillon, T., Lawrence, J.S., Meyer, C., Storey, J.W.V., Halter, B., Roth, W.L. & Walden, V. 2005. An analysis of temperatures and wind speeds above Dome C, Antarctica. *Astronomy & Astrophysics*, **430**, 739–746.

Brundt, D. 1932. Notes on radiation in the atmosphere. *Quarterly Journal of the Royal Meteorological Society*, **58**, 389–420.

Connolley, W.M. 1996. The Antarctic temperature inversion. *International Journal of Climatology*, **16**, 1333–1342.

Duarte, H.F., Dias, N.L. & Maggiotto, S.R. 2006. Assessing daytime downward longwave radiation estimates for clear and cloudy skies in Southern Brazil. *Agricultural and Forest Meteorology*, **139**, 171–181.

Dürr, B. & Philipona, R. 2004. Automatic cloud amount detection by surface longwave downward radiation measurements. *Journal of Geophysical Research*, 1029/2003JD004182.

Enomoto, H., Motoyama, H., Shiraiwa, T., Saito, T., Kameda, T., Furukawa, T., Takahashi, S., Kodama, Y. & Watanabe, O. 1998. Winter warming over dome Fuji, East Antarctica and semiannual oscillation in atmospheric circulation. *Journal of Geophysical Research*, **103**, 103–111.

Genthon, C., Town, M.S., Six, D., Favier, V., Argentini, S. & Pellegrini, A. 2010. Meteorological atmospheric boundary layer measurements and ECMWF analyses during summer at Dome C, Antarctica. *Journal of Geophysical Research*, 10.1029/2009JD012741.

Gröbner, J., Wacker, S., Vuilleumier, L. & Kämpfer, N. 2009. Effective atmospheric boundary layer temperature from longwave radiation measurements. *Journal of Geophysical Research*, 10.1029/2009JD012274.

Guest, P.S. 1998. Surface longwave radiation conditions in the eastern Weddell Sea during winter time. *Journal of Geophysical Research*, **103**, 761–771.

Hudson, R.S. & Brandt, R.E. 2005. A look at the surface-based temperature inversion on the Antarctic Plateau. *Journal of Climate*, **18**, 1673–1696.

Idso, S.B. & Jackson, R.D. 1969. Thermal radiation from the atmosphere. *Journal of Geophysical Research*, **74**, 5397–5403.

King, J.C. 1996. Longwave atmospheric radiation over Antarctica. *Antarctic Science*, **8**, 105–109.

König-Langlo, G. & Augstein, E. 1994. Parameterization of the downward long-wave radiation at the Earth's surface in polar regions. *Meteorologische Zeitschrift*, **3**, 343–347.

Lanconelli, C., Busetto, M., Dutton, E.G., König-Langlo, G., Maturilli, M., Sieger, R., Vitale, V. & Yamanouchi, T. 2011. Polar baseline surface radiation measurements during the International Polar Year 2007–2009. *Earth System Science Data*, **3**, 1–8.

Long, C.N. &, Dutton, E.G. 2002. *BSRN global network recommended QC tests*, v 2.0. Baseline Surface Radiation Network technical report. http://www.bsrn.awi.de/fileadmin/user_upload/Home/Publications/BSRN_recommended_QC_tests_V2.pdf.

Luers, J.K. 1997. Temperature errors of Vaisala rs90 radiosondes. *Journal of Atmospheric and Oceanic Technology*, **1314**, 18–29.

Ohmura, A. 1982. Climate and energy balance of the arctic tundra. *Journal of Climatology*, **2**, 65–84.

Phillpot, H.R. & Zillman, J.W. 1970. Surface temperature inversion over Antarctic continent. *Journal of Geophysical Research*, **75**, 4161–4169.

Pirazzini, R., Nardino, M., Orsini, A., Calzolari, F., Georgadis, T. & Levizzani, V. 2000. Parameterization of the downward longwave radiation from clear and cloudy skies at Ny-Ålesund (Svalbard). *In* Smith, W.L. & Timofeyev, Y.A., *eds. Current problems in atmospheric radiation*. Hampton, VA: A. Deepak, 559–562.

Ricaud, P., Genthon, C., Durand, P., Attié, J.-L., Carminati, F., Canut, G., Vanacker, J.-F., Moggio, L., Courcoux, Y., Pellegrini, A. & Rose, T. 2012. Summer to winter variabilities of temperature and water vapour in the lowermost troposphere as observed by Hamstrad over Dome C, Antartica. *Boundary Layer Meteorology*, **143**, 227–259.

Ricchiazzi, P., Shiren, Y., Gautier, C. & Sowle, D. 1998. SBDART: a research and teaching software tool for plane-parallel radiative transfer in the Earth's atmosphere. *Bulletin of the American Meteorological Society*, **576**, 2101–2114.

SWINBANK, W.C. 1963. Long-wave radiation from clear skies. *Quarterly Journal of Meteorological Society*, **89**, 339–348.

TOMASI, C., PETKOV, B., STONE, R., BENEDETTI, E., VITALE, V., LUPI, A., MAZZOLA, M., LANCONELLI, C., HERBER, A. & VON HOYNINGEN-HUENE, W. 2010. Characterizing polar atmospheres and their effect on Rayleigh-Scattering optical depth. *Journal of Geophysical Research*, 10.1029/2009JD012852.

TOWN, M.S., WALDEN, V.P. & WARREN, S.G. 2007. Cloud cover over South Pole from visual observation, satellites retrievals, and surface based infrared radiation measurements. *Journal of Climate*, **20**, 544–558.

TROSHICHEV, O., VOVK, V. & EGOROVA, L. 2008. IMF-associated cloudiness above near-pole station Vostok: impact on wind regime in Antarctica. *Journal of Atmospheric Solar-Terrestrial Physics*, **70**, 1289–1300.

UDISTI, R., DAYAN, U., BECAGLI, S., BUSETTO, M., FROSINI, D., LEGRAND, M., LUCCARELLI, F., PREUNKERT, S., SEVERI, M., TRAVERSI, R. & VITALE, V. 2012. Sea-spray aerosol in central Antarctica. Present atmospheric behaviour and implications for paleoclimatic reconstruction. *Atmospheric Environment*, **52**, 109–120.

WARREN, S.G. 1982. Optical properties of snow. *Reviews of Geophysics and Space Physics*, **20**, 67–89.

YAMANOUCHI, T. & KAWAGUCHI, S. 1984. Longwave radiation balance under a strong inversion in the katabatic wind zone, Antarctica. *Journal of Geophysical Research*, **89**, 771–778.

ZILLMAN, J.W. 1972. *A study of some aspects of the radiation and heat budgets of the Southern Hemisphere oceans. Meteorological Study* No. 26. Canberra: Bureau of Meteorology, 562 pp.